ARTICLE

Temperature Sensing Using Fluorescent Nanothermometers

Fiorenzo Vetrone,[†] Rafik Naccache,[†] Alicia Zamarrón,[‡] Angeles Juarranz de la Fuente,[‡] Francisco Sanz-Rodríguez,[‡] Laura Martinez Maestro,[§] Emma Martín Rodriguez,[§] Daniel Jaque,[§] José García Solé,[§,*] and John A. Capobianco[†,*]

[†]Department of Chemistry and Biochemistry, Concordia University, 7141 Sherbrooke Street West, Montreal, QC, H4B 1R6 Canada, [‡]Departamento de Biología, Universidad Autónoma de Madrid, Madrid 28049, Spain, and [§]GIEL, Departamento de Física de Materiales, Universidad Autónoma de Madrid, Madrid 28049, Spain

ABSTRACT Acquiring the temperature of a single living cell is not a trivial task. In this paper, we devise a novel nanothermometer, capable of accurately determining the temperature of solutions as well as biological systems such as HeLa cancer cells. The nanothermometer is based on the temperature-sensitive fluorescence of $NaYF_4$:Er^{3+},Yb^{3+} nanoparticles, where the intensity ratio of the green fluorescence bands of the Er^{3+} dopant ions ($^2H_{11/2} \rightarrow {}^4I_{15/2}$ and $^4S_{3/2} \rightarrow {}^4I_{15/2}$) changes with temperature. The nanothermometers were first used to obtain thermal profiles created when heating a colloidal solution of $NaYF_4$:Er^{3+},Yb^{3+} nanoparticles in water using a pump—probe experiment. Following incubation of the nanoparticles with HeLa cervical cancer cells and their subsequent uptake, the fluorescent nanothermometers measured the internal temperature of the living cell from 25 °C to its thermally induced death at 45 °C.

KEYWORDS: nanothermometer · upconversion · HeLa cancer cell · nanoparticles · thermal sensing

Cellular events are marked by changes in temperature.[1,2] Therefore, the ability to glean the temperature of a single living cell, especially that of a cancer cell, could have valuable repercussions leading to novel insight about its pathology and physiology, in turn, contributing to novel treatment and diagnoses. A suitable biocompatible temperature probe having minimal interactions with the cellular constituents would ascertain the effects of temperature-related processes/events including metabolic activity or thermal stress due to exogenous irradiation. Here, we report the first use of lanthanide (Ln^{3+})-doped fluorescent nanoparticles as versatile optical nanothermometers, and we show the applications of these nanoparticles in biological systems such as HeLa cancer cells.

Nanotechnology has provided new tools to sense temperature, such as nanolithography[3] or using diverse nanomaterials including carbon nanotubes (CNTs),[4,5] silver nanospheres,[6] and quantum dots (QDs).[7,8] An alternative method to sensing temperature is to use fluorescent nanomaterials or nanoparticles whose emission band shape, peak position, intensity, or lifetimes are affected by temperature.[9−12] In this context, fluorescent probes are ideal for use as cellular nanothermometers since they provide high spatial resolution at a time scale comparable to that of many cellular processes. For example, the fluorophores NBD (7-nitrobenz-2-oxa-1,3-diazol-4-yl) and Laurdan (6-dodecanoyl-2-dimethylaminonaphthalene) have been reported to accurately determine the temperature of single living cells,[13] and recently, a fluorescent hydrophilic nanogel was reported, which could determine intracellular temperatures within 0.5 °C.[14] An alternative approach is to use Ln^{3+}-doped fluorescent materials, which have shown the ability to act as thermal probes.[15−19] However, no studies of these Ln^{3+}-based probes have been performed on liquids or on biological systems. The biological uses of Ln^{3+}-doped nanoparticles (NPs) including FRET-based biosensors, *in* and *ex vivo* fluorescent imaging, as well as therapeutic applications such as photodynamic therapy have recently been demonstrated.[20−25] These NPs have attracted considerable attention since they possess the ability to emit light at higher energies than the excitation wavelengths (typically near-infrared). This multiphoton process, known as *upconversion*, is the result of doping with Ln^{3+} ions, which have "real" electronic energy states with sufficiently long lifetimes that can act as intermediaries in this process.[26] In comparison to other two-photon absorption (TPA) nanomaterials, which require cumbersome and expensive ultrafast lasers, Ln^{3+}-doped NPs can be stimulated using low power and inexpensive near-infrared (NIR) lasers. Moreover, in comparison with other types of lu-

*Address correspondence to capo@vax2.concordia.ca, jose.garcia_sole@uam.es.

Received for review February 5, 2010 and accepted April 27, 2010.

Published online May 4, 2010. 10.1021/nn100244a

minescent nanoparticles, there is no effect on the absorption/emission maxima upon varying the particle size. The upconverting nanoparticles are excited with wavelengths in the tissue penetration window (700−1000 nm), which is a necessity in the biological milieu. Unlike other types of biologically inspired NPs that are excited with high energy wavelengths, the use of NIR is advantageous on several fronts. NIR light of the appropriate wavelength is capable of deep tissue penetration, will not induce fluorescence from any fluorophore in the vicinity leading to increased resolution, and is unlikely to damage the specimen under study.[27]

In particular, fluoride-based nanoparticle matrices are receiving the most attention since the low-energy vibrations of these hosts will not deactivate the luminescence and generally results in higher luminescence efficiencies. Thus, in this paper, we demonstrate for the first time that the temperature-sensitive green emission of fluorescent $NaYF_4$:Er^{3+},Yb^{3+} NPs could be used as thermal nanoprobes for temperature sensing in liquids and HeLa cervical cancer cells.

RESULTS AND DISCUSSION

The water-dispersible PEI-capped $NaYF_4$:Er^{3+},Yb^{3+} NPs crystallize in the α-phase (cubic) with a mean particle size of *ca.* 18 nm.[23] The NPs are capable of (up)converting long-wavelength NIR light (920−980 nm) to shorter wavelengths such as green and red (Figure 1A,B). This two-photon process occurs *via* energy transfer from Yb^{3+} ions to the fluorescent Er^{3+} ions. The Yb^{3+} ions are efficient sensitizers since they possess only one excited state ($^2F_{5/2}$) that is resonant in energy with the $^4I_{11/2}$ state of Er^{3+}, the intermediate state in the process (see Figure 1A). Furthermore, it has an extinction coefficient 10-fold larger than that of Er^{3+}, although it is still orders of magnitude smaller than organic dyes and fluorophores.[28] Thus, the Er^{3+} ion is excited to its $^4F_{7/2}$ state *via* two successive transfers of energy from Yb^{3+} ions in close proximity, promoting it from its ground state ($^4I_{15/2}$) to the intermediate state ($^4I_{11/2}$) and subsequently to the excited state ($^4F_{7/2}$).[29] Figure 1B presents the emission spectrum of the erbium ion (Er^{3+}) in the green region at two different temperatures, 26 and 63 °C (λ_{exc} = 920 nm). The green emission consists of distinct bands between 515 and 535 nm (centered at 525 nm) and 535 and 570 nm (centered at 545 nm) emanating from transitions from two excited states ($^2H_{11/2}$ and $^4S_{3/2}$, respectively) to the ground state. These two states are in close proximity, essentially separated by only several hundred wavenumbers, leading to a thermal equilibrium governed by the Boltzmann factor:[30]

$$\frac{I_{525}}{I_{545}} = C\exp(-\Delta E/kT) \qquad (1)$$

where I_{525} and I_{545} are the integrated intensities of the $^2H_{11/2} \rightarrow {}^4I_{15/2}$ and $^2S_{3/2} \rightarrow {}^4I_{15/2}$ transitions, respectively,

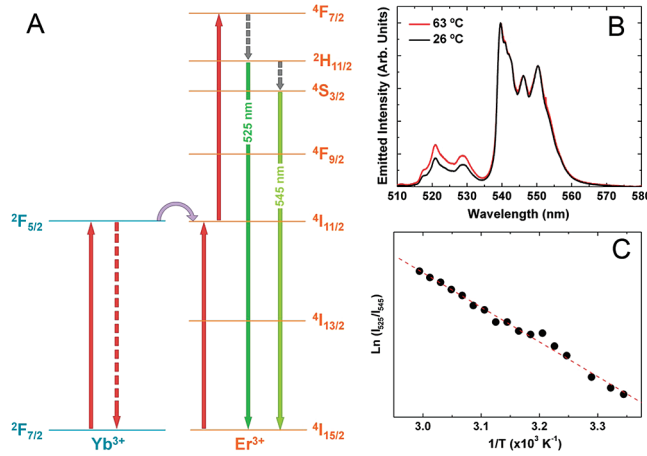

Figure 1. (A) Simplified energy level diagram showing the relevant states of the Yb^{3+} and Er^{3+} ions and the two-step upconversion excitation mechanism. The temperature sensitivity of the $NaYF_4$:Er^{3+},Yb^{3+} NPs occurs as a result of the closely spaced $^2H_{11/2}$ and $^4S_{3/2}$ energy states. (B) Upconversion emission spectra obtained at two different cuvette temperatures (λ_{exc} = 920 nm) and (C) a plot of ln(I_{525}/I_{545}) *vs* 1/*T* to calibrate the thermometric scale for the water-dispersible $NaYF_4$:Er^{3+},Yb^{3+} NPs.

C is a constant that depends on the degeneracy, spontaneous emission rate, and photon energies of the emitting states in the host materials, Δ*E* is the energy gap separating the two excited states, *k* is the Boltzmann constant, and *T* is the absolute temperature. This leads to changes in the emission intensities of these bands as a function of temperature. Thus, we can obtain a thermometric scale for the temperature-sensitive water-dispersible NPs (nanothermometers). We have systematically investigated their emission spectra at various temperatures. For this purpose, the solution was placed on a heating mount attached to a fiber-coupled confocal microscope (Olympus BX-41) connected to a high-resolution spectrometer (iHR520). The solution was optically excited at 920 nm by focusing a mode-locked Ti:sapphire laser beam (Tsunami Spectra Physics) with a low numerical aperture objective. The excitation intensity was well below 0.5 kW/cm^2 to avoid any pump-induced heating. Figure 1C shows the dependence ln(I_{525}/I_{545}) on the inverse temperature, 1/*T*. In accordance with expression 1, a linear behavior is obtained; the best fit being ln I_{525}/I_{545} = 1.74 − 1028(1/*T*) (*T* given in K). This clearly demonstrates that the temperature can be accurately measured from the ratio of the 525 and 545 nm fluorescent intensities in the temperature range relevant for most biological systems.

In solution, the $NaYF_4$:Er^{3+},Yb^{3+} NPs can be used to obtain "thermal images". The thermal gradient created through the absorption of a NIR laser beam by the solvent (water) was investigated by means of a pump−probe and confocal fluorescence microscopy experiment (Figure 2A). The same confocal system as described above was used. However, in this case, the solution was mounted on a 100 nm resolution motorized stage. It was laterally excited with a CW di-

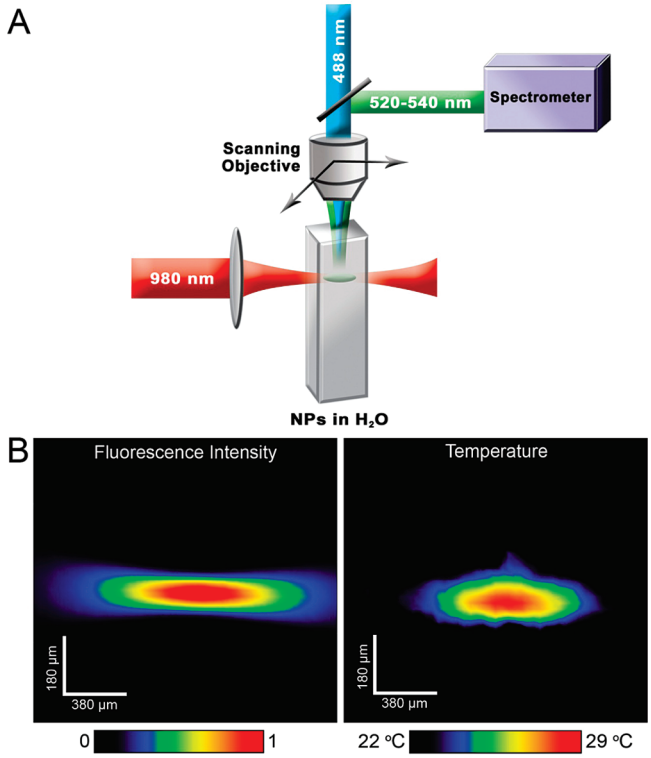

Figure 2. (A) Schematic of the pump−probe setup used to measure the temperature profile created by heating a colloidal solution of $NaYF_4:Er^{3+},Yb^{3+}$ NPs in water with a 980 nm diode laser (pump beam) and subsequently scanned with a 488 nm Ar^+ laser (probe beam). (B) Left: Confocal image of the 980 nm excited upconverted luminescence (pump absorbed profile). Right: Thermal image of the spot created by the 980 nm pump beam.

ode laser beam at 980 nm (a wavelength absorbed by water) in order to produce a temperature increase in the illuminated area as a result of water absorption. The 980 nm beam was focused into the solution by using a single lens with a numerical aperture as low as 0.2, so that optical trapping of the NPs can be neglected. This beam was also absorbed by the NPs so that the emitted upconverted visible fluorescence intensity (integrated over all the different bands) was used to reveal the pump shape profile (see Figure 2B, left panel). Simultaneously, a probe beam (Ar^+ laser beam at 488 nm, not absorbed by water) was focused into the solution orthogonally to the 980 nm pump beam. This probe beam was focused with the 10× microscope objective of the confocal system. In this way, the same objective collected the 488 nm excited luminescence generated by the NPs. The collected fluorescence was analyzed by the fiber-coupled spectrometer in order to ascertain the temperature distribution along the pumped area by monitoring the fluorescence I_{525}/I_{545} intensity ratio (Figure 2B, right panel). It can be clearly seen that the highest temperatures, approximately 30 °C, occur around the central area of illumination (focal point), where the 980 nm absorption (upconverted luminescence) is highest. At the same time, a temperature gradient was observed from the non-illuminated area (around 22 °C) to the central area of illumination (close to 30 °C). Thus, the ability of the $NaYF_4:Er^{3+},Yb^{3+}$ fluorescent NPs to record thermal gradient images of liquids is clearly manifested.

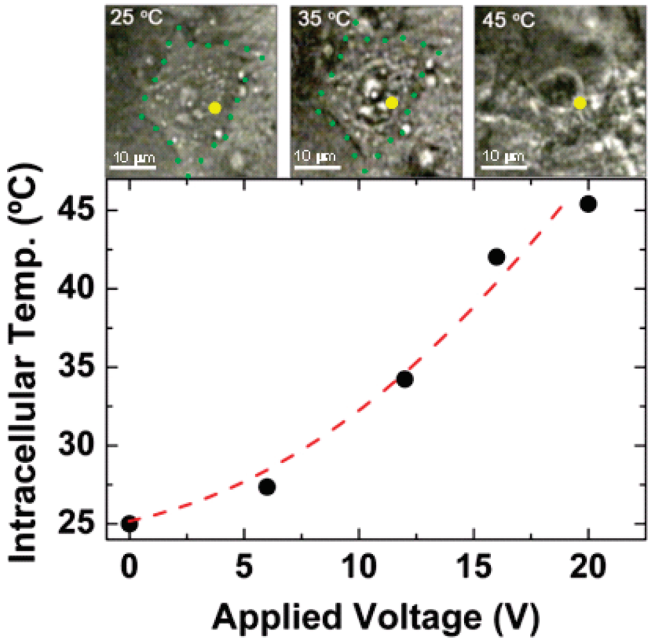

Figure 3. (Top) Optical transmission images of an individual HeLa cell at three inner temperatures. Cell death is observed at 45 °C. (Bottom) Temperature of the HeLa cell determined by the Er^{3+} ion fluorescence in the $NaYF_4:Er^{3+},Yb^{3+}$ NPs as a function of the applied voltage.

The $NaYF_4:Er^{3+},Yb^{3+}$ NPs were subsequently incorporated in a biological system in order to investigate their thermometric ability. In previous work, we have shown that the $NaYF_4:Er^{3+},Yb^{3+}$ NPs can be internalized quite efficiently by cervical cancer cells (HeLa).[23] It is therefore feasible to exploit the thermal sensitivity of the $^2H_{11/2}$ and $^4S_{3/2}$ bands to create a nanothermometer capable of measuring the internal temperature of a living cancer cell. Thus, immortalized human carcinoma cells were incubated for 1.5 h with the nanothermometers, and the room temperature optical transmission image of an individual HeLa cell was obtained. The cells were placed in the confocal microscope described above. In this case, the excitation beam (920 nm) was focused with a 50× microscope objective into the point marked in the transmission image of Figure 3 (in yellow) so that the upconverted (Er^{3+}) fluorescence of the NPs permitted the measurement of the inner HeLa cell temperature (25 °C). The temperature of the cell was varied by means of a metallic platform connected to a resistor such that the cell temperature could be varied by changing the applied voltage. The I_{525}/I_{545} intensity ratio of the nanothermometers changed with the applied voltage and permitted measurement of the internal temperature of the illuminated HeLa cell at each corresponding voltage (Figure 3). The observed quadratic dependence is reasonable since the Joule dissipated energy varies with the square of the applied voltage. Therefore, we are able to investigate the cellular changes occurring as a result of the external heating

by means of transmission optical images of the illuminated cells at different temperatures (Figure 3). At room temperature (25 °C), the cancer cells show an irregular shape, typical of such cells (green dotted outline). A subsequent temperature increase to 35 °C does not produce any relevant changes in its morphology. However, increasing the temperature to 45 °C, a small membrane fragment was observed, which is indicative of cell death.

It is important to point out that these fluorescent NPs could be used as dual-mode probes by providing a means to not only measure the cellular temperature but also impart the ability to image the cell. Effectively, this points toward the versatility of such a multimodal system, which possesses several advantages over other fluorophores.

In summary, we have shown that fluorescent $NaYF_4$:Er^{3+},Yb^{3+} NPs can be successfully used as nanothermometers. The ratio between the $^2H_{11/2} \rightarrow {}^4I_{15/2}$ and $^2S_{3/2} \rightarrow {}^4I_{15/2}$ emissions of the Er^{3+} ion provides an optical method to measure temperature distributions (temperature gradients) in liquids by means of confocal fluorescence. We have also shown the biological usefulness of these nanothermometers by measuring temperature changes of an individual cancer cell up to its thermally induced death.

METHODS

Synthesis of $NaYF_4$:Er^{3+},Yb^{3+} Nanoparticles. The $NaYF_4$:Er^{3+},Yb^{3+} NPs (2 mol % of Er^{3+}, 18 mol % of Yb^{3+}, respectively) were synthesized *via* a solvothermal process.[23] In a typical experiment, 3.6 mmol of NaCl (99.99%, Aldrich), 1.44 mmol of $YCl_3 \cdot 6H_2O$ (99.99%, Aldrich), 0.036 mmol of $ErCl_3 \cdot 6H_2O$ (99.995%, Aldrich), and 0.324 mmol of $YbCl_3 \cdot 6H_2O$ (99.998%, Aldrich) were dissolved in a 27 mL solution of ethylene glycol (99+%, Aldrich) containing 0.45 g of branched polyethylenimine (M_w ~25 000, Aldrich) and stirred for approximately 60 min. Subsequently, a solution of 17 mL of ethylene glycol with 7.2 mmol of NH_4F (99.99+%, Aldrich) was added to the initial solution containing the chlorides and stirred for another 30 min. The resulting clear solution was then placed in a 250 mL Teflon-lined autoclave (Berghof/America) and heated with stirring for 24 h at 200 °C. The resulting NPs were isolated *via* centrifugation and washed twice with distilled water and ethanol. The NPs were then dried under vacuum for 24 h. A 1 wt % colloidal dispersion in water was prepared for all spectroscopic measurements.

X-ray Powder Diffraction (XRPD) Analysis. XRPD patterns were measured using a Scintag XDS-2000 diffractometer equipped with a Si(Li) Peltier-cooled solid-state detector, Cu Kα source at a generator power of 45 kV and 40 mA, divergent beam (2 and 4 mm), and receiving beam slits (0.5 and 0.2 mm). Scan range was set from 20 to 80° 2θ with a step size of 0.02° and a count time of 2 s. The sample was measured using a quartz "zero background" disk.

Transmission Electron Microscopy (TEM) and Selected Area Electron Diffraction (SAED). TEM measurements of the colloidal dispersion of NPs were performed with a Philips CM200 microscope operating at 200 kV equipped with a charge-coupled device (CCD) camera (Gatan). A minute amount of sample was dispersed in an appropriate amount of water to yield an approximate 0.1 wt % solution. A drop of the resulting solution was evaporated on a Formvar/carbon film supported on a 300 mesh copper grid (3 mm in diameter).

Spectroscopy and Fluorescence Microscopy. Visible emission from the $NaYF_4$:Er^{3+},Yb^{3+} NPs was obtained upon excitation with three different lasers, a 980 nm CW diode laser, a Spectra Physics Tsunami fs Ti-sapphire pulsed laser (100 fs, 920 nm, and 80 MHz repetition rate), and a CW Ar^+ ion laser at 488 nm. Images were obtained with a confocal fluorescence microscope (Olympus BX-41) using a 50× objective with a numerical aperture of 0.75. The microscope was also used to record optical transmission images in order to allow for precise location of the excitation spot on the sample (cell or cuvette). For spectral analysis, the collected emitted light was focused into a fiber connected to a high-resolution spectrometer (iHR520). Temperature variation of the samples (cell or cuvette) was carried out by controlling the electric power dissipated by a resistor attached to the sample.

Acknowledgment. This work was supported by the Universidad Autónoma de Madrid and Comunidad Autonoma de Madrid (Projects CCG087-UAM/MAT-4434 and S2009/MAT-1756), by the Spanish Ministerio de Educacion y Ciencia (MAT 2007-64686), and by a Banco Santander-CEAL-UAM project. The authors also thank the Natural Sciences and Engineering Research Council (NSERC) of Canada and the Gouvernement du Québec, Ministère du Développement économique, de l'Innovation et de l'Exportation for funding. J.G.S. thanks the Spanish Minsterio de Educación for financial support for a research stay at Concordia University (ref PR2009-0040).

REFERENCES AND NOTES

1. Suzuki, M.; Tseeb, V.; Oyama, K.; Ishiwata, S. Microscopic Detection of Thermogenesis in a Single HeLa Cell. *Biophys. J.* **2007**, *92*, L46–L48.
2. Zohar, O.; Ikeda, M.; Shinagawa, H.; Inoue, H.; Nakamura, H.; Elbaum, D.; Alkon, D. L.; Yoshioka, T. Thermal Imaging of Receptor-Activated Heat Production in Single Cells. *Biophys. J.* **1998**, *74*, 82–89.
3. Lee, J.; Kotov, N. A. Thermometer Design at the Nanoscale. *Nano Today* **2007**, *2*, 48–51.
4. Dorozhkin, P. S.; Tovstonog, S. V.; Golberg, D.; Zhan, J.; Ishikawa, Y.; Shiozawa, M.; Nakanishi, H.; Nakata, K.; Bando, Y. A Liquid Ga-Filled Carbon Nanotube: A Miniaturized Temperature Sensor and Electrical Switch. *Small* **2005**, *1*, 1088–1093.
5. Gao, Y.; Bando, Y. Carbon Nanothermometer Containing Gallium. *Nature* **2002**, *415*, 599.
6. Lan, Y.; Wang, H.; Chen, X.; Wang, D.; Chen, G.; Ren, Z. Nanothermometer Using Single Crystal Silver Nanospheres. *Adv. Mater.* **2009**, *21*, 4839–4844.
7. Han, B.; Hanson, W. L.; Bensalah, K.; Tuncel, A.; Stern, J. M.; Cadeddu, J. A. Development of Quantum Dot-Mediated Fluorescence Thermometry for Thermal Therapies. *Ann. Biomed. Eng.* **2009**, *37*, 1230–1239.
8. Walker, G. W.; Sundar, V. C.; Rudzinski, C. M.; Wun, A. W.; Bawendi, M. G.; Nocera, D. G. Quantum-Dot Optical Temperature Probes. *Appl. Phys. Lett.* **2003**, *83*, 3555–3557.
9. Binnemans, K. Lanthanide-Based Luminescent Hybrid Materials. *Chem. Rev.* **2009**, *109*, 4283–4374.
10. Engeser, M.; Fabbrizzi, L.; Licchelli, M.; Sacchi, D. A Fluorescent Molecular Thermometer Based on the Nickel(II) High-Spin/Low-Spin Interconversion. *Chem. Commun.* **1999**, 1191–1192.
11. Löw, P.; Kim, B.; Takama, N.; Bergaud, C. High-Spatial-Resolution Surface-Temperature Mapping Using Fluorescent Thermometry. *Small* **2008**, *4*, 908–914.
12. Wang, S.; Westcott, S.; Chen, W. Nanoparticle Luminescence Thermometry. *J. Phys. Chem. B* **2002**, *106*, 11203–11209.
13. Chapman, C. F.; Liu, Y.; Sonek, G. J.; Tromberg, B. J. The Use of Exogenous Fluorescent Probes for Temperature Measurements in Single Living Cells. *Photochem. Photobiol.* **1995**, *62*, 416–425.

14. Gota, C.; Okabe, K.; Funatsu, T.; Harada, Y.; Uchiyama, S. Hydrophilic Fluorescent Nanogel Thermometer for Intracellular Thermometry. *J. Am. Chem. Soc.* **2009**, *131*, 2766–2767.
15. Aigouy, L.; Tessier, G.; Mortier, M.; Charlot, B. Scanning Thermal Imaging of Microelectronic Circuits with a Fluorescent Nanoprobe. *Appl. Phys. Lett.* **2005**, *87*, 184105-1–184105-3.
16. Alencar, M. A. R. C.; Maciel, G. S.; de Araújo, C. B.; Patra, A. Er^{3+}-Doped $BaTiO_3$ Nanocrystals for Thermometry: Influence of Nanoenvironment on the Sensitivity of a Fluorescence Based Temperature Sensor. *Appl. Phys. Lett.* **2004**, *84*, 4753–4755.
17. Allison, S. W.; Gillies, G. T.; Rondinone, A. J.; Cates, M. R. Nanoscale Thermometry *via* the Fluorescence of YAG:Ce Phosphor Particles: Measurements from 7 to 77 °C. *Nanotechnology* **2003**, *14*, 859–863.
18. Wade, S. A.; Collins, S. F.; Baxter, G. W. Fluorescence Intensity Ratio Technique for Optical Fiber Point Temperature Sensing. *J. Appl. Phys.* **2003**, *94*, 4743–4756.
19. Yap, S. V.; Ranson, R. M.; Cranton, W. M.; Koutsogeorgis, D. Decay Time Characteristics of La_2O_2S:Eu and La_2O_2S:Tb for Use within an Optical Sensor for Human Skin Temperature Measurement. *Appl. Opt.* **2008**, *47*, 4895–4899.
20. Chatterjee, D. K.; Rufaihah, A. J.; Zhang, Y. Upconversion Fluorescence Imaging of Cells and Small Animals Using Lanthanide Doped Nanocrystals. *Biomaterials* **2008**, *29*, 937–943.
21. Hilderbrand, S. A.; Shao, F.; Salthouse, C.; Mahmood, U.; Weissleder, R. Upconverting Luminescent Nanomaterials: Application to *In Vivo* Bioimaging. *Chem. Commun.* **2009**, 4188–4190.
22. Jiang, S.; Zhang, Y.; Lim, K. M.; Sim, E. K. W.; Ye, L. NIR-to-Visible Upconversion Nanoparticles for Fluorescent Labeling and Targeted Delivery of siRNA. *Nanotechnology* **2009**, *20*, 155101/1–155101/9.
23. Vetrone, F.; Naccache, R.; Juarranz de la Fuente, A.; Sanz-Rodríguez, F.; Blazquez-Castro, A.; Martín Rodriguez, E.; Jaque, D.; García Solé, J.; Capobianco, J. A. Intracellular Imaging of HeLa Cells By Non-Functionalized $NaYF_4$:Er^{3+},Yb^{3+} Upconverting Nanoparticles. *Nanoscale* **2010**, *2*, 495−498.
24. Wang, F.; Liu, X. Recent Advances in the Chemistry of Lanthanide-Doped Upconversion Nanocrystals. *Chem. Soc. Rev.* **2009**, *38*, 976–989.
25. Wang, M.; Mi, C.-C.; Wang, W.-X.; Liu, C.-H.; Wu, Y.-F.; Xu, Z.-R.; Mao, C.-B.; Xu, S.-K. Immunolabeling and NIR-Excited Fluorescent Imaging of HeLa Cells by Using $NaYF_4$:Yb,Er Upconversion Nanoparticles. *ACS Nano* **2009**, *3*, 1580–1586.
26. Auzel, F. Upconversion and Anti-Stokes Processes with f and d Ions in Solids. *Chem. Rev.* **2004**, *104*, 139–173.
27. König, K. Multiphoton Microscopy in Life Sciences. *J. Microsc.* **2000**, *200*, 83–104.
28. Vetrone, F.; Naccache, R.; Mahalingam, V.; Morgan, C. G.; Capobianco, J. A. The Active-Core/Active-Shell Approach: A Strategy To Enhance the Upconversion Luminescence in Lanthanide-Doped Nanoparticles. *Adv. Funct. Mater.* **2009**, *19*, 2924–2929.
29. Tikhomirov, V. K.; Driesen, K.; Rodriguez, V. D.; Gredin, P.; Mortier, M.; Moshchalkov, V. V. Optical Nanoheater Based on the $Yb^{3+}-Er^{3+}$ Co-doped Nanoparticles. *Opt. Express* **2009**, *17*, 11794–11798.
30. Saïdi, E.; Samson, B.; Aigouy, L.; Volz, S.; Löw, P.; Bergaud, C.; Mortier, M. Scanning Thermal Imaging by Near-Field Fluorescence Spectroscopy. *Nanotechnology* **2009**, *20*, 115703/1–115703/8.